Research article

Enhancing catalyst stability: Immobilization of Cu–Fe catalyst in sodium alginate matrix for methyl orange removal via Fenton-like reaction

Pongpanit Kongkoed [a], Natthaphong Lertna [a], Pakpoom Athikaphan [a], Athit Neramittagapong [a,b], Sutasinee Neramittagapong [a,b,*]

[a] Department of Chemical Engineering, Faculty of Engineering, Khon Kaen University, Khon Kaen, 40002, Thailand
[b] Research Center for Environmental and Hazardous Substance Management (EHSM), Khon Kaen University, Khon Kaen, 40002, Thailand

A R T I C L E   I N F O

A B S T R A C T

This study aims to enhance the stability and effectiveness of heterogeneous catalysts in Fenton-like reactions, explicitly addressing the acidity limitations inherent in traditional Fenton processes. Copper-iron was synthesized through co-precipitation, and a catalyst bead was produced from hydrogel formation. X-ray diffraction (XRD) and X-ray photoelectron spectroscopy (XPS) confirm phases in the bimetallic Copper-iron, aligning with the intended composition. Modification with alginate led to reduced metal leaching compared to the bare bimetallic counterpart, as confirmed by atomic absorption spectroscopy (AAS). Additionally, Fourier-transform infrared spectroscopy (FTIR) revealed the deactivation of alginate through the disappearance of carboxyl groups, indicating the depolymerization of the catalyst bead. Under the suggested conditions (Methyl Orange concentration of 25 mg/L, initial solution pH of 7, 2 g/L catalyst loading, concentration of hydrogen peroxide 100 mM in a 120-min reaction time), the catalyst demonstrated remarkable decolorization efficiency of Methyl Orange, achieving 97.67 %. Further highlighting its practicality, the catalyst exhibited outstanding reusability over four cycles under identical conditions, showcasing robust immobilization capabilities and sustained performance. Notably, the catalyst's magnetic properties facilitated easy separation using an external magnet. In conclusion, the developed catalyst beads offer a solution with high reusability, magnetic separability, and reduced iron leaching. The advantageous characteristics underscore its potential as a heterogeneous catalyst for wastewater treatment applications, warranting further exploration under practical conditions.

1. Introduction

In recent decades, the widespread use of dyes in industries such as textiles, food, and pharmaceuticals has enhanced product value and appearance. However, it has also resulted in the discharge of harmful pigments into the environment, necessitating water treatment [1]. In recent years, various approaches have been explored to address this issue. Biological treatment, for example, has proven effective but often requires extended treatment times and involves complex procedures [2]. Flocculation-coagulation methods

---

have also been employed; however, they tend to generate substantial amounts of residual sludge post-treatment [3]. Additionally, adsorption techniques have been utilized, but these methods necessitate the disposal of spent sorbents and regeneration solutions, and the desorption of pollutants from these sorbents is not always successful. Despite their limitations, these processes have been instrumental in mitigating dye toxicity [4]. However, these methods often produce secondary pollutants that require further treatment. As a result, there has been a surge in research focused on effective methods for removing organic pollutants from water [5,6]. Advanced oxidation processes (AOPs) are increasingly acknowledged as viable approaches for decomposing contaminants, especially within industries such as pesticide manufacturing, paper production, and textile dyeing [7–10]. Among AOPs, the Fenton reaction stands out for its simplicity and efficacy [11,12]. In the classical Fenton reaction, Fe^{2+} generates hydroxyl radicals (•OH), which play an important role in pollutant degradation. Despite its advantages, the Fenton reaction is hindered by high acidity requirements (pH ~3), iron sludge formation, and metal leaching, which pose sustainability and environmental challenges in water treatment processes [13]. Numerous researchers have explored heterogeneous catalysts to overcome these drawbacks, aiming for reaction reusability [14, 15]. However, these catalysts still operate under acid conditions, presenting a persistent challenge in achieving a more sustainable and environmentally friendly water treatment approach [16,17].

A few researchers have proposed using transition metals such as Cu [18] Mn [19] and Ag [20] in a Fenton-like reaction for pollutant. Recently, The Cu metal has been shown the high effective because it can be utilized in wider pH range [18]. Sriprom et al. (2023) have successfully decomposed lignin using Cu/MCM-41 in the Fenton-like reaction, with the activity increasing at higher pH levels due to the role of copper [21]. Numerous studies have endeavored to improve catalyst performance by synthesizing Cu–Fe bimetal composites, a pursuit aimed at augmenting catalytic activity. This undertaking poses a substantial challenge in mitigating the conventional drawbacks associated with Fenton reactions [22]. The intricate synthesis of Cu–Fe bimetal is envisioned not only as a means to bolster catalyst efficacy but also as a strategic response to address the inherent limitations of classical Fenton methodologies. In various heterogeneously catalyzed reactions, bimetal catalysts have outperformed their metal counterparts in terms of catalytic performance. Nguyen et al. (2020) studied a Fe–Cu composite, finding that the optimal mass ratio of Fe^{3+}: Fe^{2+}: Cu^{2+} was 2:1:0.3. Their study suggested that a higher copper concentration enhances catalyst activity by promoting the generation of •OH radicals. The composite exhibited high catalytic activity at a pH of 7 and maintained effectiveness across a wide range of pH conditions [23]. However, a slight decrease in mineralization was observed due to metal leaching, which resulted in the loss of active sites in the solution. Consequently, modifications to the Fe–Cu composite are necessary to reduce metal leaching and maintain its catalytic efficiency.

Several studies have explored incorporating bimetallic composites onto support matrices, where the catalyst comprises two metals. These bimetallic composites have been shown to enhance catalytic activity and potentially reinforce catalyst stability [19,24,25]. Furthermore, they exhibit superior catalytic performance compared to single-metal catalysts. Several studies have specifically reported on the effectiveness of bimetallic catalysts in Fenton-like reactions. Wang et al. (2015) employed CuFe/MC (Mesoporous Carbon) over the Fenton-like reaction in removing 100 mg/L bisphenol (BPA). Their findings revealed that, under best conditions of 25 °C, a catalyst loading of 0.3 g/L, 30 mM H_2O_2, and a pH of 3, CuFe/MC demonstrated an impressive BPA removal rate of approximately 93 %. Furthermore, CuFe can display better catalytic activity than monometallic of Cu and Fe [24]. Similarly, Karthikeyan et al. (2016) have investigated CuFe supported on SBA-15 catalyst to decompose N, N-diethyl-p-phenyl diamine (DPD). Their results indicated an 83 % removal at the 0.1 g/L CuFe/SBA-15, 8 mM H_2O_2, and a pH 4 [26]. However, they noted effectiveness was limited to acidic pH levels (pH 3), and metal leaching was observed in the solution. In response to this challenge, researchers explored hydrogel as a catalyst support. Previous research has underscored the effectiveness of hydrogel as a suitable support for heterogeneous catalysts, with alginate demonstrating notable efficacy in minimizing mass loss during the reuse of bead catalysts [27]. The application of hydrogels as catalyst supports has generated significant interest. Alginate, an extensively studied hydrogel, stands out for its exceptional support properties, ensuring uniform metal distribution and reducing mass loss in subsequent catalyst reuse [28].

In the scope of this work, Cu and Fe bimetal were synthesized by co-precipitation and incorporated into an alginate matrix, resulting in the creation of (Cu–Fe)/Alg beads via a hydrogel method. These beads were then utilized as catalysts in the Fenton-like reaction for the MO removal, with particular emphasis on evaluating their reusability and catalytic efficiency. The significance of this study is in creating a new Cu–Fe catalyst using co-precipitation. This catalyst showed better performance than single-metal catalysts, working efficiently at neutral pH. It also demonstrated excellent reusability by reducing metal leaching after the reaction, indicating its potential for practical use in wastewater treatment with reduced environmental impact.

2. Material and methods

2.1. Chemicals

Methyl orange dye ($C_{14}H_{14}N_3NaO_3S$) was procured from KemAus. Ferric chloride ($FeCl_3 \cdot 6H_2O$) was obtained from Panreac Applichem, Spain, while sodium hydroxide (NaOH, 99 %) and calcium chloride dihydrate ($CaCl_2 \cdot 2H_2O$) were sourced from RCI Labscan. Nitric acid (HNO_3, 65 wt%) was acquired from Merck (Germany). Additionally, hydrogen peroxide (H2O2, 30 wt%), copper (II) chloride dihydrate ($CuCl_2 \cdot 2H_2O$, 99 %), and iron (II) sulfate ($FeSO_4 \cdot 7H_2O$, 98 %) were obtained from Ajax Finechem Pty, Ltd. Notably, sodium alginate ($[(C_6H_7O_6Na)_n$, 5–40 cps at 1%w in water 25 °C) was employed. In contrast, all aqueous solutions were prepared with deionized (DI) water.

2.2. Co-precipitation of Cu–Fe powder

Cu–Fe powder was synthesized using the co-precipitation method, according to the procedure reported by Nguyen et al. [23]. Briefly, stock solutions of 0.5 M FeCl$_3$·6H$_2$O, 0.1 M CuCl$_2$·2H$_2$O, and 0.2 M FeSO$_4$·7H$_2$O were prepared. Subsequently, 10 mL aliquots of each solution were mixed and stirred to ensure uniformity. The resultant solution was gently dropped into 5 M NaOH in 150 mL. The mixture was left for an hour, during which solid particles formed and remained suspended in the solution. Afterward, the mixture was separated by centrifugation at 4500 rpm to isolate the solid particles. Once separated, the solid particles were rinsed and centrifuged several times with ethanol and DI water until the supernatant was clear. Finally, the suspended solid was dried in an oven at 90 °C overnight to provide the Cu–Fe powder.

Additionally, monometallic samples such as copper (Cu) and iron (Fe) powder were synthesized using the same procedure to serve as comparison metals for evaluating catalytic activity. For example, Fe was synthesized from a solution consisting of 0.5 M FeCl$_3$·6H$_2$O and 0.2 M FeSO$_4$·7H$_2$O. Then, 10 mL of each solution was gently mixed and added dropwise into a 5 M NaOH solution. The suspended solids were formed and separated using the centrifugal method. The collected solids were washed and dried using the same method as Cu–Fe powder. Similarly, Cu powder was prepared from a 0.1 M CuCl$_2$·2H$_2$O solution, with 10 mL added dropwise into a 5 M NaOH solution. The subsequent separating, washing, and drying steps were conducted in the same manner as described previously.

2.3. Preparation of catalyst bead using hydrogel method

The catalyst bead was synthesized via the hydrogel method, as described in reference. [27] Sodium alginate (SA) 1 g and DI 100 g were meticulously mixed with the Cu–Fe under rigorous stirring conditions. The resulting catalyst, designated as [X-(Cu–Fe)/Alg], adhered precisely to the specifications outlined in Table 1. The variable 'X' denotes the mass ratio of the Cu–Fe powder to sodium alginate, with values ranging from x = 0:1 to 1:1, and all samples are based on 1 g SA. To ensure uniform distribution of Cu–Fe powder, the solution underwent ultrasonication for 30 min. The sonicated solution was slowly dropped into a 5 % w/v CaCl$_2$·2H$_2$O solution with a solution volume of 100 mL to form uniform solid beads with a diameter of 3 mm. Subsequently, the formed bead catalyst was immersed overnight in a 5 % w/v CaCl$_2$·2H$_2$O solution in 100 mL to promote complete crosslinking within the polymer matrix. Alginate and Ca^{2+} ions interacted to prevent the leaching of included elements, such as the Cu–Fe, and to strengthen the stability of the beads [29]. For comparative analysis, (0.10)-Cu/Alg and (0.10)-Fe/Alg catalyst beads were synthesized using the same methodology as seen in Table 1. These monometallic catalysts were utilized to investigate potential synergistic effects arising from the integration of the Cu–Fe powder.

2.4. Characterization of Cu–Fe/Alg catalyst

The phase structure of the Cu–Fe powder was synthesized from co-precipitation. It was analyzed using X-ray diffraction (XRD) using an EMPYREAN XRD Instrument (PANalytical, Netherlands) with Cu Kα radiation (wavelength of 0.15406 nm). The analysis spanned the 2θ range from 5° to 100°, with an exact step size of 0.01°. Al K radiation was used as the excitation source for X-ray photoelectron spectroscopy (XPS), ascertaining the catalysts' oxidation state. Notably, binding energy at 284.8 eV for C1s peak was used to calibrate XPS measurements at BL5.3 SUTNANOTEC-SLRI at the Synchrotron Light Research Institute (SLRI) in Thailand. Confirming the Cu–Fe powder was synthesized using the co-precipitation method. To determine the textural properties of the Cu–Fe powder and catalyst bead, the N$_2$ adsorption-desorption technique. Isotherms were employed. N$_2$ adsorption isotherms were measured at saturated temperature (−196 °C) using a micromeritics device (ASAP2460, USA). Cu–Fe powder and catalyst bead were degassed under vacuum at 150 °C for 4 h. The surface (S$_{BET}$) and pore size diameter of the catalyst bead and Cu–Fe powder were determined using the Brunauer-Emmett-Teller (BET) and Barrett-Joyner-Halenda (BJH) methods, respectively. The determination of the metal loading was accomplished using atomic absorption spectroscopy (AAS); 0.1 g of the samples, which were Cu–Fe powder and catalyst bead, underwent digestion utilizing the acid digestion method, and the catalyst bead reusability test examined the possibility of metal leaching. Attenuated Total Reflectance (ATR) mode in the 550 and 4500 cm^{-1} range from FTIR was applied to identify the functional group of both catalyst bead and Cu–Fe powder. A scanning electron microscope (SEM) was used to reveal the catalyst bead surface structure and element mapping through energy-dispersive X-ray Spectroscopy (EDS).

Table 1
Catalyst bead composition: Sodium alginate mixed with Cu–Fe.

Catalysts	Metallic content (g)	SA content (g)	Mass ratio
Cu–Fe	1.00	0	1.00:0
SA	0	1	0:1
0.10-(Cu)/Alg	0.10 (Cu)	1	0.10:1
0.10-(Fe)/Alg	0.10 (Fe)	1	0.10:1
0.10-(Cu–Fe)/Alg	0.10	1	0.10:1
0.25-(Cu–Fe)/Alg	0.25	1	0.25:1
0.50-(Cu–Fe)/Alg	0.50	1	0.50:1
0.75-(Cu–Fe)/Alg	0.75	1	0.75:1
1.00-(Cu–Fe)/Alg	1.00	1	1.00:1

2.5. Fenton-like reaction

Methyl Orange (MO) degradation via a Fenton-like reaction was conducted in a batch reactor employing a shaker set to 100 rpm to facilitate mixing during the reaction. A 0.2 g catalyst bead was introduced into a 250 mL conical flask containing a MO concentration of 25 mg/L in 100 mL.

To systematically evaluate the catalyst's efficacy, the experiments varied the metal loading [X-(Cu–Fe)-Alg; X = 0, 0.1, 0.25, 0.50, 0.75, 1], H_2O_2 concentration (ranging from 10 to 1000 mM), and the solution's pH (adjusted between 3 and 11). Acidic pH was achieved using 0.1 M HNO_3, while alkaline conditions were adjusted with 0.1 M NaOH.

Adsorption tests were initially conducted by placing 100 mL of an MO dye aqueous solution in contact with a specific dose of catalyst beads in a flask, which was then agitated using an orbital shaker at 100 rpm for 120 min. The dye concentration was monitored throughout the adsorption process until a stable saturation value was reached. It was observed that after 60 min, the MO concentration remained unchanged. Therefore, we decided to immerse the catalyst in the MO solution for 60 min before starting all experiments.

In a typical Fenton-like reaction, H_2O_2 was added to the solution, and samples were collected at 1, 10, 15, 30, 60, and 120 min. Subsequently, 1 mL of each sample was filtered using a 0.22-μm syringe filter. The MO concentration at each sampling time was determined by colorimetry using a UV–vis spectrophotometer. Calibration curves were developed for each pH condition from 3 to 11 to accurately measure the MO concentration at different pH levels. The percentage of MO removal was calculated according to Equation (1).

$$Y = \frac{C_0 - C_t}{C_0} \times 100\% \tag{1}$$

Where Y is the percentage of MO removal.

C_0 is the initial concentration of MO (mg/L)

C_t is the concentration of MO (mg/L) at time t.

The catalyst bead was separated from the aqueous solution using an external magnet and filtration, which was subsequently utilized in the reaction to assess catalyst reusability. Before doing more runs, the catalyst bead was washed with DI. These meticulous experimental procedures ensure a thorough evaluation of the bead catalyst's efficacy in MO degradation.

It is important to ensure that the catalyst can be used multiple times for the process to be practical. In our study, we conducted four consecutive experiments using the same catalyst beads. After each treatment, we retrieved the beads using a magnet, washed them with distilled water, and then dried them. These experiments were performed under consistent optimal conditions.

3. Results and discussion

3.1. Catalyst bead characterization

The X-ray diffraction (XRD) patterns of the studied phase structure revealed characteristic diffraction peaks at 2θ angles, indicative of their crystalline structures. These peaks were subsequently associated with corresponding crystallographic planes of the materials. The XRD pattern of Cu–Fe powder is shown in Fig. 1, in which Cu–Fe was synthesized from the co-precipitation method. The XRD pattern of Cu_2O exhibited distinct peaks at 2θ angles of 29.7°, 52.7°, and 61.6°, corresponding to the crystallographic planes [0 1 1], [1 2 1], and [0 2 2], respectively. This pattern is consistent with the known crystal structure of cuprous oxide (JCPDS Card No. 96-101-0927). Similarly, the XRD pattern of Fe_2O_3 displayed peaks at 2θ angles of 24.1°, 33.2°, 35.6°, 39.3°, 40.9°, 49.5°, 54.1°, 62.4°, and 63.9°, associated with the crystallographic planes [1 0−2], [1 0 4], [1 1 0], [0 0 6], [1 1 3], [2 0−4], [1 1 6], [2 1 4], and [3 0 0], respectively, consistent with the known characteristics of hematite (α-Fe_2O_3), (JCPDS Card No. 96-210-1170). Furthermore, the XRD

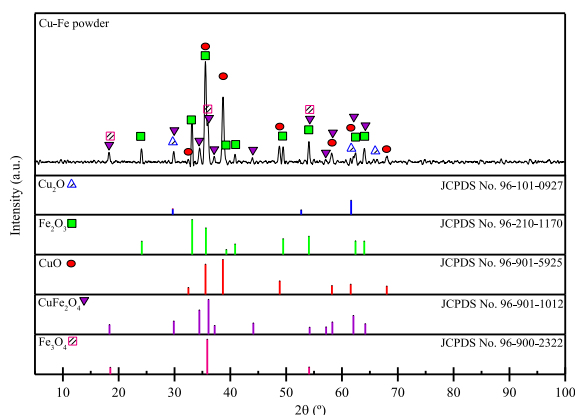**Fig. 1.** XRD patterns of Cu–Fe powder.

pattern of CuO exhibited peaks at 2θ angles of 32.5°, 35.5°, 38.7°, 48.8°, 58.2°, 61.5°, and 66.4°, corresponding to the crystallographic planes [1 1 0], [−1 1 1], [1 1 1], [−2 0 2], [2 0 2], [−1 1 3], and [3 1 0], respectively, consistent with the metal structure of copper (II) oxide (JCPDS Card No. 96-901-5925). Additionally, the XRD pattern of Fe_3O_4 exhibited peaks at 2θ angles of 18.5°, 35.9°, and 54.1° corresponding to the crystallographic planes [1 1 1], [1 3 1], and [2 4 2] respectively, consistent with the inverse spinel structure of magnetite (JCPDS Card No. 96-900-2322). Furthermore, the XRD pattern of $CuFe_2O_4$ revealed peaks at 2θ angles of 18.4°, 29.9°, 34.4°, 36.1°, 37.2°, 44.1°, 54.2°, 57.2°, 58.3°, 62.1°, and 64.2° corresponding to the crystallographic planes [1 0 1], [1 1 2], [1 0 3], [2 1 1], [2 0 2], [0 0 4], [3 1 2], [3 0 3], [3 2 1], [2 2 4], and [4 0 0], respectively, consistent with the spinel structure of copper iron oxide (JCPDS Card No. 96-901-1012). The results were confirmed by XPS to validate the oxidation state of the Cu–Fe powder.

The Cu–Fe powder was inspected using XPS spectra to discover the oxidation states of Cu, Fe, and O. The survey spectrum of this catalyst was depicted in Fig. 2a, showing distinct peaks corresponding to Cu, Fe, and O. XPS spectra of Cu2p, Fe2p, and O1s using the Lovlentz method unveiled the nuanced characteristics of the Fe element. The Fe2p spectrum underwent deconvolution (Fig. 2b), identifying distinct orbitals of Fe^{2+} at 709.8 eV ($2p_{3/2}$) and 723.9 eV ($2p_{1/2}$), along with Fe^{3+} at 711.1 eV ($2p_{3/2}$) and 712.5 eV ($2p_{3/2}$) and 725.7 eV ($2p_{1/2}$). This identification was further affirmed by satellite peaks at 719.2 eV [30]. The XPS spectrum of Cu2p (Fig. 2c) The deconvoluted peaks in the XPS spectra of Cu2p identified distinct orbitals of Cu^+ at 952.2 eV ($2p_{1/2}$) and 932.4 eV ($2p_{3/2}$), along with Cu^{2+} at 953.2 eV ($2p_{1/2}$) and 933.7 eV ($2p_{3/2}$). This identification is further affirmed by satellite peaks at 942.8 and 940.4 eV [31]. Fe_3O_4, Fe_2O_3, Cu_2O, CuO, and $CuFe_2O_4$ all include different valence states and chemical environments of Fe and Cu, which are compatible with the XRD data. The peaks produced by the deconvolution of O1s (Fig. 2d) can be used to verify the formula of metal. The peaks appear at 529.5 eV, 530.7 eV, and 531.9 eV, corresponding to C═O/C–O, –OH, and Metal-O. It is noteworthy that both the Fe and Cu oxides exhibit metal bonding, as indicated by the peak at 531.9 eV [32]. These detailed XPS analyses provide a nuanced understanding of the composition, oxidation states, and chemical environments within the Cu–Fe powder catalyst.

AAS analysis was used to determine the metal content in the catalyst beads. As shown in Table 2, the metal content increases noticeably with higher ratios. The incorporation of Cu–Fe powder into alginate was carefully evaluated using AAS, and the detailed findings are documented in Table 2. Importantly, the values for Fe and Cu show an increase with higher metal loading, indicating the successful synthesis of the X-(Cu–Fe)-Alg catalysts within the hydrogel matrix. After incorporating the Cu–Fe powder into the alginate matrix, it was observed that both the concentrations of Cu and Fe increased as the metal content increased. This resulted in a consistent Cu and Fe ratio close to 1:5 across all samples. These findings provide important information about the metal composition and distribution in the produced X-(Cu–Fe)-Alg catalysts.

The FTIR analysis elucidated the shifts in chemical bonds resulting from varying Cu–Fe loading on alginate. Fig. 3 presents the FTIR spectra of Cu–Fe loaded into alginate by mass ratio alongside bare Cu–Fe. The broad band observed at 3600~3200 cm^{-1} in the FTIR spectra of alginate and X-(Cu–Fe)/Alg; X = 0.1–1.0 can be attributed to the stretching vibration of the abundant hydroxyl group (-OH) in sodium alginate. The peaks at 1600 and 1400 cm^{-1} in the spectra of alginate and X-(Cu–Fe)/Alg correspond to the vibrations of asymmetric and symmetric C–O–C, as reported [36,37]. Additionally, in the spectrum of bare Cu–Fe, the peaks at 1448 and 1126 cm^{-1} indicate metal-hydroxide (Metal-OH; Fe–OH/Cu–OH) vibrations [38,39], while the peaks at 883 and 788 cm^{-1} are attributed to iron
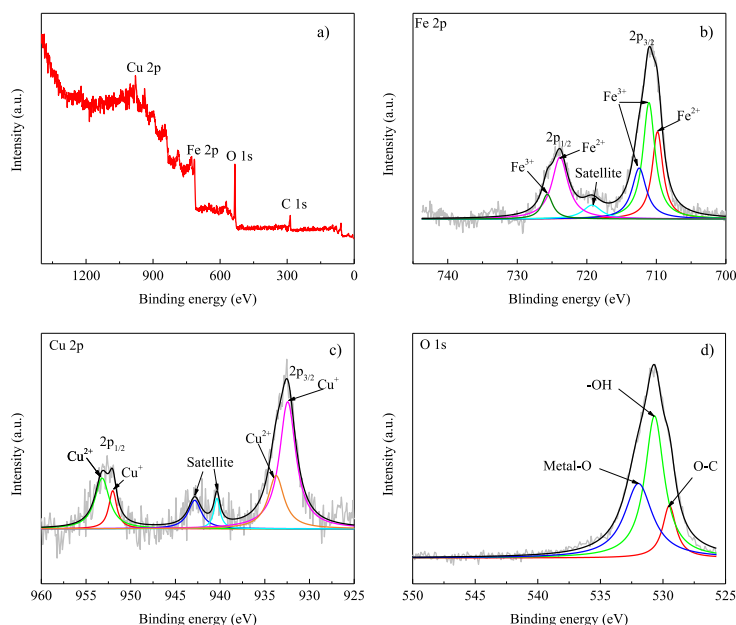

Fig. 2. XPS spectra of Cu–Fe a) survey spectrum, b) Cu2p, c) Fe2p, and d) O1s.

Table 2
Physicochemical Parameters of the Cu–Fe and X-(Cu–Fe)/Alg catalysts.

Catalysts	Cu content[a] (mg/g_{cat})	Fe content[a] (mg/g_{cat})	BET surface[b] area (m^2/g_{cat})	Pore volume[b] (cm^3/g_{cat})	Pore size[b] (nm)
Cu–Fe	88.63	434.45	67.49	0.2297	13.61
SA	0	0	2.04	0.0011	2.11
0.10-(Cu–Fe)/Alg	4.98	31.86	2.51	0.0050	13.32
0.25-(Cu–Fe)/Alg	12.73	69.04	3.14	0.0197	16.03
0.50-(Cu–Fe)/Alg	21.72	122.01	3.36	0.0109	18.62
0.75-(Cu–Fe)/Alg	28.71	158.37	3.60	0.0173	19.23
1.00-(Cu–Fe)/Alg	41.99	225.47	5.86	0.0237	16.14

[a] Analyzed using atomic absorption spectroscopy.

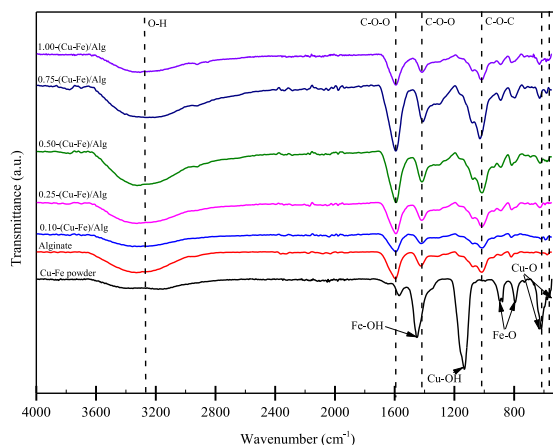[b] Analyzed using N$_2$ adsorption-desorption.

Fig. 3. FTIR spectra of x-(Cu–Fe)/Alg, where x = 0–1.0.

oxide (Metal-O; Fe–O), and those at 622 and 558 cm^{-1} denote copper oxide (Metal-O; Cu–O) [40,41]. Upon investigating potential interactions in the FTIR spectra of Cu–Fe loaded into alginate by mass ratio, it was observed that high Cu–Fe loading exhibited more stretching vibration bands at 1600 and 1400 cm^{-1}, indicating increased polymer cross-linkage [42,43]. Notably, the shape and intensity of the C–O–O group were visibly altered, suggesting that the carboxyl group of alginates may serve as a binding site for coordination bonding with Cu-Fe [37]. Furthermore, peaks at 1488, 1126, 883, 788, and 558 cm^{-1}, assigned to Metal-OH and Metal-O of
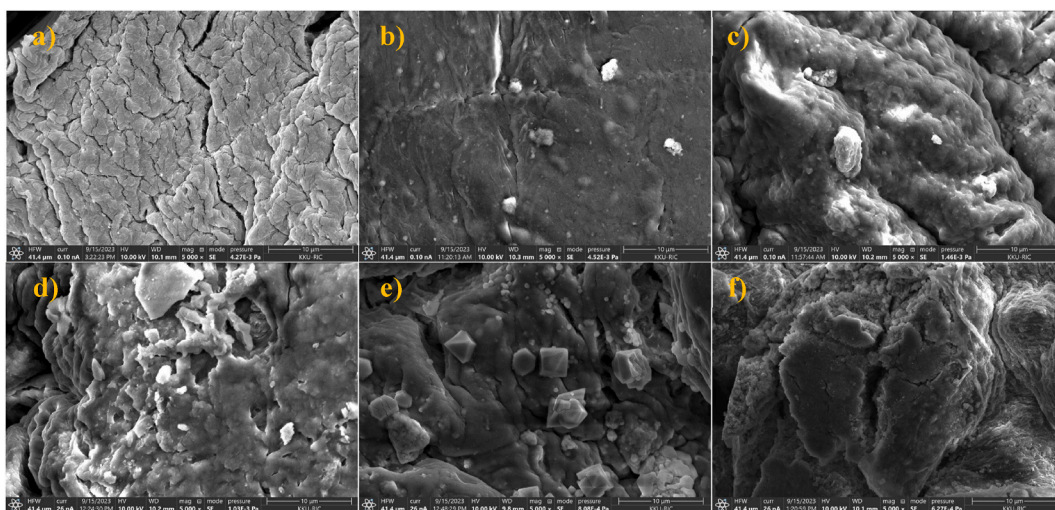

Fig. 4. SEM image and EDS mapping of Fe and Cu element a) Alginate b) 0.10-(Cu–Fe)-Alg, c) 0.25-(Cu–Fe)-Alg, d) 0.50-(Cu–Fe)-Alg, e) 0.75-(Cu–Fe)-Alg, and f) 1.00-(Cu–Fe)-Alg.

bare Cu–Fe powder, disappeared in X-(Cu–Fe)/Alg with the addition of Cu–Fe powder into alginate. This disappearance can be attributed to the oxidized Cu–Fe possessing hydroxyl groups and binding with the hydroxyl groups, indicative of alginate binding onto Cu–Fe via carboxylate and hydroxyl groups [44]. As depicted in Fig. 3, the peak corresponding to C–O–O exhibited an increase with higher metal mass ratios. However, intriguingly, the 1.00-(Cu–Fe)/Alg configuration demonstrated a lower C–O–O peak than the 0.75-(Cu–Fe)/Alg counterpart. This observation suggests alginate may not adequately immobilize the metal within its matrix at higher loading ratios. Consequently, this discrepancy could potentially influence the structural integrity of alginate and weaken the bonding between Cu–Fe powder and alginate. Moreover, the presence of metal blocking within the alginate matrix was apparent, which could have implications for catalytic activity.

The SEM analysis conducted at 5000× magnification provided insights into the surface characteristics of the catalyst. Fig. 4a) depicting Alginate, only the surface of the alginate polymer without metal loading was observed. No discernible particles were identified, indicating polymer cross-linking. Conversely, in Fig. 4b) 0.10-(Cu–Fe)/Alg, metal particles were evident on the surface following loading, manifesting as darkened regions within the polymer matrix. Bright particles observed alongside were attributed to metal entities. This phenomenon was absent in Fig. 4a), highlighting the effect of metal loading. As the Cu–Fe powder mixing ratio increased, Fig. 4c–f) revealed a proportional augmentation in metal particle presence. However, in Fig. 4f) 1.00-(Cu–Fe)/Alg, a notable accumulation of metal particles was observed, indicating particle agglomeration. The conspicuous clustering of bright particles on the alginate surface suggested that metal particles were primarily situated on the surface rather than encapsulated within the alginate matrix. This aggregation likely hindered pollutant and H_2O_2 transportation through metal blockage of pores, thereby reducing catalytic activity. Consequently, the 1.00-(Cu–Fe)/Alg activity was inferior to 0.75-(Cu–Fe)/Alg. Based on SEM findings, the 0.75-(Cu–Fe)/Alg catalyst ratio is recommended due to its optimal metal particle dispersion. Moreover, the dye degradation activity surpassed that of Alginate, 0.10-(Cu–Fe)/Alg, 0.25-(Cu–Fe)/Alg, 0.50-(Cu–Fe)/Alg, and 1.00-(Cu–Fe)/Alg configurations. Subsequent SEM-EDS analysis was performed to investigate further the surface properties of the 0.75-(Cu–Fe)/Alg catalyst.

The SEM and EDS mapping of 0.75-(Cu–Fe)/Alg provide an intricate insight into the elemental composition, encompassing C, O, Ca, Cu, and Fe (Fig. 5a–f). The EDS spectrum, depicted in Fig. 5g, delineates the proportions within the 0.75-(Cu–Fe)/Alg catalyst, comprising 6.3 wt% C, 36.7 wt% O, 18.2 wt% Ca, 28.4 wt% Fe, and 10.4 wt% Cu. Furthermore, Fig. 5b–f showcases EDS mapping, highlighting the effective dispersion of Fe and Cu within the Alginate matrix. The Fe/Cu ratio on the surface is approximately 3 based on SEM-EDS, while AAS indicates a Fe/Cu ratio of around 5.5. This difference is due to the different methods used: SEM-EDS directly examines the catalyst surface, whereas AAS requires the catalyst to be dissolved for analysis. The dissolution process in AAS may lead to a higher metal ratio than EDS. Therefore, the differences observed between AAS and EDS analyses result from the variations in analytical methods. Additionally, this result confirms that alginate can immobilize the metal on the surface and within the matrix.

The presence of the C element highlights the role of the alginate polymer in helping to attach the metal to the surface. The abundance of O in the spectrum indicates compounds within the catalyst, showing that O is prevalent in the alginate due to
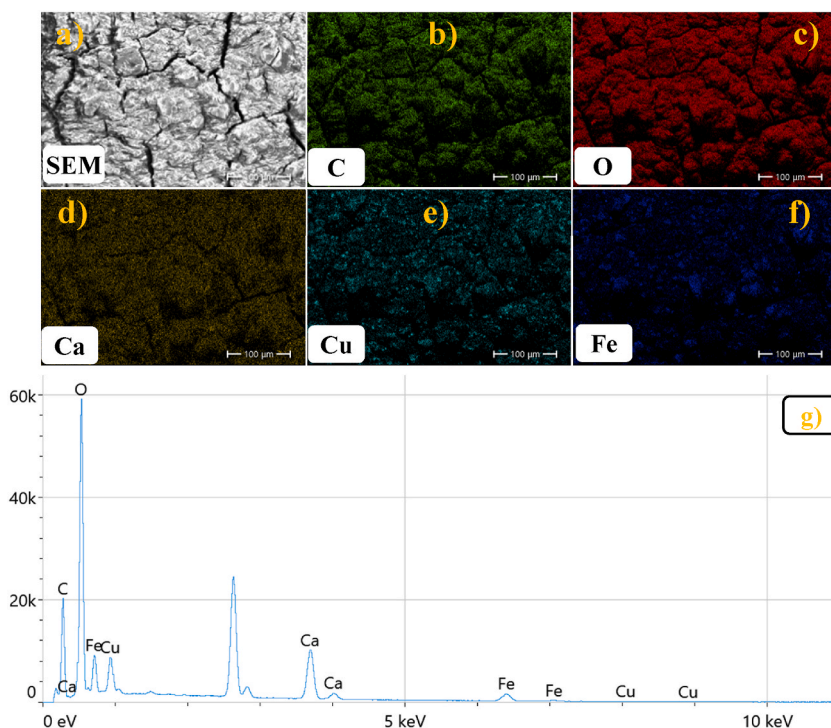

Fig. 5. Scanning Electron Microscopy and Elemental Mapping of 0.75-(Cu–Fe)-Alg catalyst. (a) SEM image (b) Element mapping of C, (c) O, (d) Ca, (e) Cu, (f) Fe; (g) EDS spectrum of 0.75-(Cu–Fe)-Alg.

functionalization, such as COO-, C–O–C, and –OH. This suggests that the observed metal may exist as metal oxide or hydroxide. Additionally, the Ca elements play a crucial role in cross-linking the polymer, assisting in the attachment of the metal [29].

The specific locations of Cu and Fe on the alginate, as shown in Fig. 5e–f, can be observed in the metal dispersed on the surface of the polymer, with no metal agglomeration observed. These thorough investigations provide a comprehensive understanding of the distribution and interaction of various components within the 0.75-(Cu–Fe)/Alg catalyst.

N_2 adsorption-desorption isotherms of Cu–Fe powder, Alginate, and 0.75-(Cu–Fe)/Alg are provided in Fig. 6a, b, and 6c, respectively. From the BET and Barrett-Joyner-Halenda (BJH) analysis, the surface area, pore volume, and pore size of Cu–Fe were found to be 67.49 m^2/g$_{cat}$, 0.2297 cm^3/g$_{cat}$, and 13.61 nm, respectively [33]. The materials can be classified as microporous (pore size <2 nm), mesoporous (2 nm < pore size <50 nm), and macroporous (pore size >50 nm) [34]. Therefore, Cu–Fe powder was classified as mesoporous due to a pore size falling between 2 nm and 50 nm. Moreover, the Type IVb isotherms exhibited by Cu–Fe powder indicate conical and cylindrical mesopores closed at the tapered end, leading to type H2(b) hysteresis according to the IUPAC classification [34, 35]. This type of hysteresis loop suggests a narrow distribution of pore bodies with a wide neck size distribution. Fig. 6b) illustrates the case of desorption via cavitation. The 0.75-(Cu–Fe)/Alg is provided in Fig. 6c), where the adsorption and desorption curves do not coincide with the hysteresis loop. The type of hysteresis loop is connected to specific pore structures and underlying adsorption process characteristics [34,35]. Hysteresis is present in a type IV(a) isotherm and capillary condensation, occurring when the pore width suppresses a critical width [33]. H2(a) hysteresis loop suggests some ordered porous nature of 0.75-(Cu–Fe)/Alg. The surface area, pore volume, and pore size of 0.75-(Cu–Fe)/Alg were 3.60 m^2/g$_{cat}$, 0.0173 cm^3/g$_{cat}$, and 19.23 nm, respectively. The mesoporous nature of 0.75-(Cu–Fe)/Alg is suggested by the pore size falling between 2 nm and 50 nm. The specific surface area of 0.75-(Cu–Fe)/Alg was lower than that of Cu–Fe powder due to the encapsulation of Cu–Fe powder into a gel matrix by an alginate polymer, which inherently exhibits a low specific surface area [29]. However, compared to pure alginate-based polymers (Figs. 6b), 0.75-(Cu–Fe)/Alg demonstrates a better specific surface area due to the adding Cu–Fe powder within the hydrogel. Furthermore, the pore size of 0.75-(Cu–Fe)/Alg was higher than that of pure alginate-based polymers. It has been found that the specific surface area of 0.75-(Cu–Fe)/Alg was lower than that of 1.00-(Cu–Fe)/Alg due to the higher metal loading in the latter, which improved the specific surface area but also led to metal aggregation on the catalyst bead surface, as observed in SEM images. While 1.00-(Cu–Fe)/Alg exhibited higher metal loading, resulting in observable metal aggregation on the surface, 0.75-(Cu–Fe)/Alg demonstrated greater
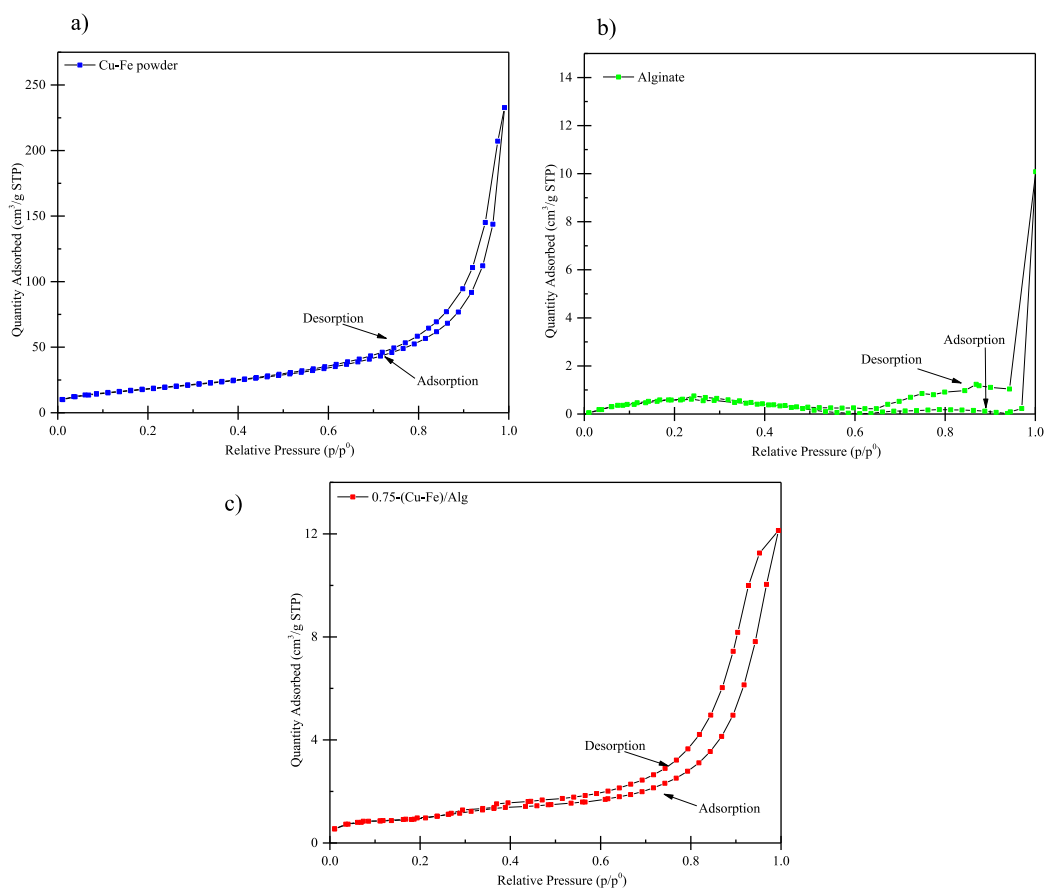

Fig. 6. N_2 adsorption-desorption curve of a) Cu–Fe powder, b) Alginate, and c) 0.75-(Cu–Fe)/Alg.

metal dispersion compared to 1.00-(Cu–Fe)/Alg. The abundant pores and moderate surface area of 0.75-(Cu–Fe)/Alg foster enhanced interaction between H_2O_2 and methyl orange, amplifying the catalytic activity observed in the pronounced degradation during a Fenton-like reaction. This effect is attributed to the optimal metal loading within 0.75-(Cu–Fe)/Alg.

3.2. Catalytic performances of Cu–Fe/Alg catalysts for MO removal

The synergistic effect between copper (Cu) and iron (Fe) was evidenced through our experimental design. Our catalyst, synthesized via co-precipitation and subsequently formed into beads, employed an Alginate-based polymer. Denoted as 0.10-(Fe)/Alg, 0.10-(Cu)/Alg, and 0.10-(Cu–Fe)/Alg, these encapsulated Fe, Cu, and Cu–Fe within Alginate, respectively, were utilized for degrading methyl orange (MO) in a Fenton-like reaction. All catalyst beads were subjected to identical conditions: MO concentration at 25 mg/L, a volume of 100 mL, a catalyst dosage of 2 g/L, H_2O_2 concentration of 100 mM, and pH 7. Fig. 7 illustrates the correlation between C/C_0 and time. The dye concentration was monitored throughout the adsorption process until a stable saturation value was reached. Remarkably, only H_2O_2 was added to the MO solution to detect degradation; MO with H_2O_2 alone showed negligible degradation (15.3 %). Similarly, degradation was minimal (7.9 %) after 120 min when MO degradation was tested without chemical additives. Upon evaluating the adsorption equilibrium of the (Cu–Fe)/Alg catalyst, it exhibited an adsorption percentage of 23.7 within 60 min. This adsorption major occurred on the surface, bolstered by Alginate's naturally hydrophilic groups, enhancing its adsorption capabilities [45]. The degradation of MO commenced post-adsorption by the addition of an H_2O_2 concentration of 100 mM. The results demonstrated that 0.10-Fe/Alg and 0.10-Cu/Alg achieved MO degradation percentages of 36.6 and 43.1, respectively. A comparison between the two indicated that 0.10-Cu/Alg exhibited superior efficacy over 0.10-Fe/Alg in degrading MO, with the difference attributed to the neutral pH 7 conditions. Notably, Fe exhibited reduced catalytic activity at pH 7, as reported by (Ozbey Unal et al., 2019), utilizing Fe_3O_4, where increased pH resulted in decreased decolorization [46]. Conversely, 0.10-Cu/Alg demonstrated an efficient reaction, resulting in favorable MO degradation. As reported by Singh et al. (2016), Cu on zeolite exhibited improved degradation of Congo red with increased pH, with the optimum pH at 7 [18]. On the other hand, the 0.10-(Cu–Fe)/Alg catalyst achieved the highest degradation, reaching 53.6 %, owing to the synergistic effect between Fe and Cu within Cu–Fe. Nguyen et al. (2020) studied the synthesis and analysis of Fe–Cu catalysts, revealing that increased Cu loading facilitated increased active sites, resulting in enhanced degradation [23]. Thus, using 0.10-(Cu–Fe)/Alg can address the limitations of Fenton-like reactions: 1. Overcoming homogeneous catalysts with heterogeneous ones and 2. Operating effectively under neutral pH (7), further study is required to explore factors affecting additional degradation.

3.3. Effect of H_2O_2 concentration on methyl orange degradation

The pivotal role of H_2O_2 as the radical source in Fenton-like processes for pollutant removal is widely acknowledged. As a potent oxidizing agent in the presence of iron and copper, H_2O_2 is integral to driving these reactions forward [47]. However, achieving an effective and economically viable Fenton-like process necessitates better control over H_2O_2 dosages. Our objective in this experiment was to determine the optimal conditions for a Fenton-like process, specifically focusing on maximizing performance through precise H_2O_2 dosage control using 0.10-(Cu–Fe)/Alg catalyst. We investigated the impact of varying H_2O_2 concentrations, specifically at 10 mM and 1000 mM, while maintaining catalyst dosage at 2 g/L and pH 7, as depicted in Fig. 8. The results revealed a correlation between degradation efficiency and reaction time. Notably, we observed a significant enhancement in methyl orange degradation efficiency, from 34.5 % to 52.7 %, with an increase in H_2O_2 concentration from 10 to 100 mM after 120 min of reaction time. On the
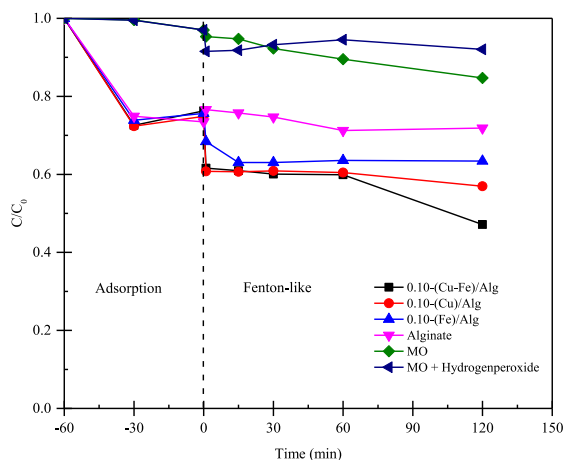

Fig. 7. MO degradation over catalyst bead; Alg, 0.10-(Cu–Fe)/Alg, 0.10-Cu/Alg, 0.10-Fe/Alg, and blank via Fenton-like reaction at pH 7, Catalyst Loading of 2 g/L, 100 mM H_2O_2 and MO 25 mg/L in 100 mL, and 120 min.
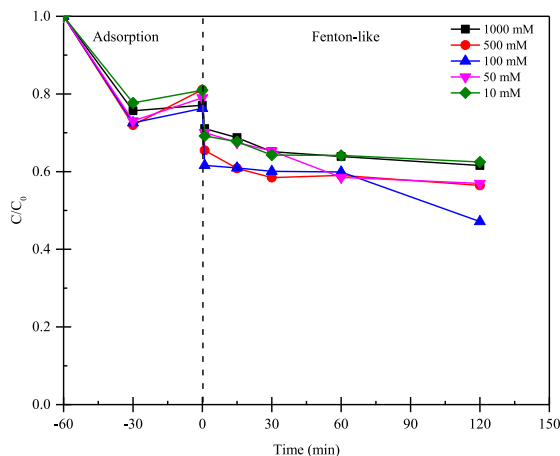
Fig. 8. The Influence of H_2O_2 on the removal of MO using a Fenton-like reaction was investigated over 0.10-(Cu–Fe)/Alg catalyst with 2 g/L catalyst loading, pH 7, and H_2O_2 concentrations ranging from 10 to 1000 mM at an MO concentration of 25 mg/L.

other hand, with further escalation of H_2O_2 concentration from 100 to 500 mM, we observed a significant decrease in MO degradation efficiency, from 52.7 % to 43.6 %. Remarkably, at an H_2O_2 concentration of 1000 mM, degradation efficiency decreased by 14.3 %, indicating a scavenger effect. This phenomenon can be attributed to the scavenging of •OH radicals by excess H_2O_2, resulting in the formation of less reactive hydroperoxyl radicals (•OOH) [48], thereby impeding methyl orange degradation. Thus, the optimum H_2O_2 dosage for achieving the highest degradation efficiency was determined to be 100 mM. In conclusion, our findings advocate for the best H_2O_2 dosage of 100 mM as the optimal condition for methyl orange degradation in a Fenton-like reaction. Excessive H_2O_2 concentrations risk overwhelming the reaction system, reducing pollutant oxidation. Therefore, we advocate for caution and recommend adherence to the 100 mM H_2O_2 concentration for optimal pollutant removal in Fenton-like reactions.

3.4. Effect of Cu–Fe loading on methyl orange degradation

The number of active sites on alginate-based polymer was crucial in methyl orange removal, but it was always a bottleneck. In this work, we anticipated that combining alginate-based polymer and Cu–Fe may obtain functional active sites that were beneficial for degrading methyl orange in a Fenton-like reaction. As depicted in Fig. 9, the methyl orange removal efficiency of 0.75-(Cu–Fe)/Alg (95.79 %) was higher than Alginate (28.12 %), 0.10-(Cu–Fe)/Alg (59.09 %), 0.25-(Cu–Fe)/Alg (61.29 %), 0.50-(Cu–Fe)/Alg (62.68 %), and 1.00-(Cu–Fe)/Alg (64.36 %). The results indicate the importance of Cu–Fe loading in alginate metrics. The catalytic capabilities of alginate-based polymer were strengthened with the incorporation of Cu–Fe content, indicating that alginate-based polymer contained more active sites.

However, it can be seen that 1.00-(Cu–Fe)/Alg showed lower activity than 0.75-(Cu–Fe)/Alg due to the high metal loading that
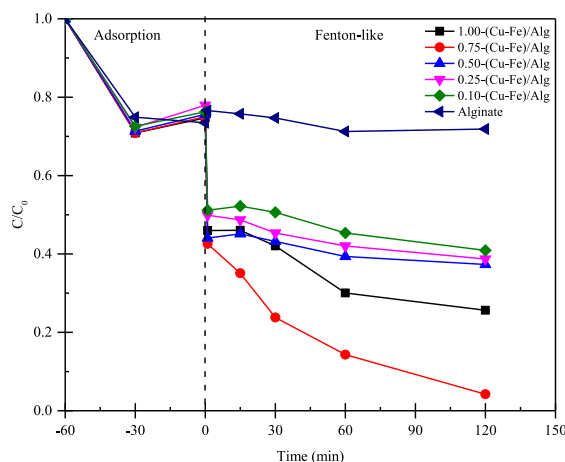

Fig. 9. Effect of Cu–Fe loading on MO removal via Fenton-like Reaction at Initial MO 25 mg/L, Catalyst Loading of 2 g/L, pH 7, 100 mM H_2O_2, and 120 min.

affects the encapsulation of alginate to Cu–Fe. From Table 2 shows the BET and Barrett–Joyner–Halenda (BJH) analysis of the surface area, pore volume, and pore size of Alginate, 0.10-(Cu–Fe)/Alg, 0.25-(Cu–Fe)/Alg, 0.50-(Cu–Fe)/Alg, 0.75-(Cu–Fe)/Alg, and 1.00-(Cu–Fe)/Alg. Additionally, from BJH pore size distribution, it was found that pore sizes between 2 and 19 nm were present in all samples. X-(Cu–Fe)/Alg was illustrated as mesoporous. Moreover, when adding the Cu–Fe powder into an alginate-based polymer. The trend of specific surface area was increased. Conversely, increasing the metal loading from 0.10-(Cu–Fe)/Alg to 0.75-(Cu–Fe)/Alg increased pore size diameter. However, at 1.00-(Cu–Fe)/Alg, the pore size diameter decreased due to the excessive metal loading. The decrease in pore size was attributed to metal aggregation, as observed in the SEM image of 1.00-(Cu–Fe)/Alg. This indicates that the metal covered the alginate, causing the aggregation, which reduced catalytic activity during the Fenton-like reaction with 1.00-(Cu–Fe)/Alg. Therefore, a metal loading ratio of 0.75-(Cu–Fe)/Alg is appropriate for achieving high catalytic activity in MO removal. Furthermore, the FTIR spectrum at 1.00-(Cu–Fe)/Alg shows a shrink of C–O–O, which is assigned to the carboxyl group of C–O–C, revealing the cross-linking of the polymer contraction. The cross-linking of the polymer was decreased due to the shrinkage of C–O–C. It also indicates that the incomplete metal immobilization on alginate [43,48] Besides, it might be blocked or deactivated by the accumulation of reaction intermediates on the surface of the catalyst bead. Furthermore, the excessive metal loading can lead to the agglomeration of metal nanoparticles within the alginate matrix. Therefore, combined with the above results together, the alginate-based polymer doped with the proper Cu–Fe content [0.75-(Cu–Fe)/Alg] was selected for further studies.

3.5. Effect of pH on methyl orange degradation

The Fenton-like reaction's efficiency is intricately linked to the pH level, significantly influencing the generation of •OH radicals crucial for the reaction. To explore this dependency, we investigated the impact of pH solutions ranging from 3 to 11 on methyl orange (MO) degradation via the Fenton-like reaction, as illustrated in Fig. 10. At a pH of 11, we observed a notably weak MO degradation of 37.8 %. This finding aligns with previous research by Nguyen et al. (2020) [23], which demonstrated that in basic conditions, H_2O_2 undergoes spontaneous decomposition, resulting in reduced availability for the reaction and consequently diminishing dye degradation. This observation corroborates our findings at pH 11, where the lowest dye degradation was observed. Conversely, at pH levels ranging from 3 to 7, MO degradation exceeded 95 %. Under these conditions, the catalyst beads effectively facilitated the production of •OH radicals essential for MO removal. However, when the pH was raised to 9, a notable decline in degradation efficiency was observed compared to the pH range of 3–7. At pH 9, MO degradation was recorded at 87.3 %. This decline can be attributed to the high pH (pH 9) hindering the further reaction between Fe^{2+} and H_2O_2. Additionally, Cu may occupy the active sites, thereby reducing MO removal efficiency at around pH 9. This behavior aligns with the findings of the Fe and Cu catalysts [18]. Traditionally, the Fenton reaction operates optimally under acidic conditions, typically around pH 3, as this pH range supports the necessary reaction between Fe^{2+} and H_2O_2 to generate radicals [49]. However, applying this system to MO removal presents a challenge, as maintaining such acidic conditions can be impractical. Using catalyst beads provides a practical solution to overcome this challenge, allowing for the conduct of the Fenton-like reaction at near-neutral pH levels.

3.6. Kinetics study

To determine the degradation kinetic of methyl orange (MO) on a catalyst bead using a Fenton-like process, the pseudo-first-order and pseudo-second-order kinetic models were examined under the conditions of a MO concentration of 25 mg/L, a hydrogen peroxide concentration of 100 mM, and a 0.75-(Cu–Fe)/Alg of 2 g/L. The absorbance of the detected compound is proportional to its concentration according to the Lambert-Beer equation, and as such, the absorbance can be used in the rate expression instead of
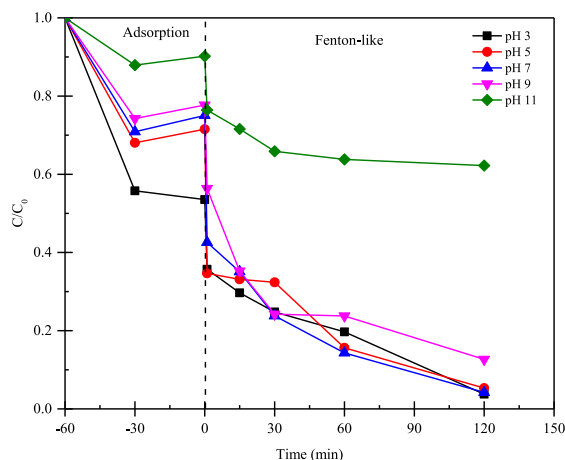

Fig. 10. Effect of initial solution pH on MO degradation. Reaction conditions: 0.75-(Cu–Fe)/Alg catalyst, Catalyst Loading of 2 g/L, 100 mM H_2O_2, and reaction time of 120 min.

concentration [50].The degradation kinetics of MO by the Fenton-like process was studied at different contact times varying from 1 to 120 min. Assuming pseudo-first-order reaction kinetics for MO dye removal, the rate constant, k, was computed from the slope of the logarithmic plot of concentration (C) versus contact time (t) as presented in Equation (2). The plot is shown in Fig. 11a).

$$\text{Pseudo} - \text{First} - \text{order } \ln\left(\frac{C}{C_0}\right) = -k_1 t \tag{2}$$

$$\text{Pseudo} - \text{Second order } \frac{1}{C} = k_2 t + \frac{1}{C_0} \tag{3}$$

Where C is a concentration of MO (mg/L) at a time.

C_0 is the initial concentration of MO (mg/L)

k is the rate constant

t is time (min)

The pseudo-second-order rate constant was obtained from the plot of t/C_t versus t as presented in Equation (3). The plot is shown in Fig. 11b). The data obtained are presented in Table 3. In order to fit the best experimental data, the correlation coefficients of both models were compared. The rate constants obtained from the kinetics plots of the pseudo-first-order model were higher than the pseudo-second-order model. Thus, the results of the experiments indicated that the degradation of MO dye by a Fenton-like process could be best described by the pseudo-first-order kinetic model. Moreover, the rate constant is 0.0196 min^{-1}.

3.7. Treatment cost estimation and catalyst reusability

A series of experiments determined the conditions for achieving the highest methyl orange (MO) degradation. These experiments utilized a 100 mL solution with an initial 25 mg/L MO concentration. The catalyst employed was a bead catalyst [0.75-(Cu–Fe)/Alg] at a dosage of 2 g/L. Additionally, the solution contained a hydrogen peroxide (H$_2$O$_2$) concentration of 100 mM and an initial pH of 7. The selection of pH 7 was based on its neutrality and the consistent degradation observed across various pH levels (3, 5, 7, and 9). Under these best conditions, the catalyst bead exhibited exceptional performance, achieving approximately 97.67 % removal of MO.

A simplified cost estimation using analytical grade chemicals was necessary for this study. The electricity and unit operations costs were considered negligible, as the focus was solely on the chemical treatment and synthesis of catalysts. The treatment process cost for removing MO (25 mg/L) per liter and the capital cost of the chemicals were estimated based on cost per kilogram. As shown in Table 4, the wastewater treatment cost is $4.20 per liter. This cost is divided into two main components: catalyst synthesis and reaction cost. Catalyst synthesis accounts for 98 % of the total cost, while the reaction cost is around 2 %. The high cost of catalyst synthesis is due to using analytical-grade chemicals. Therefore, future research should focus on improving the synthesis method to reduce engineering costs.

The reusability potential of 0.75-(Cu–Fe)/Alg and Cu–Fe powder was assessed based on their catalytic performance and framework stability over four consecutive cycles. As shown in Table 5, 0.75-(Cu–Fe)/Alg achieved approximately 97 % performance in MO removal for the first cycle, whereas Cu–Fe powder achieved around 45 %. This higher activity of 0.75-(Cu–Fe)/Alg is due to the encapsulation of Cu–Fe powder within alginate, which enhances catalytic activity. The hydrophilic nature of alginate aids in transferring the oxidizing agent within its structure to react with the metal. Cheng et al. observed that hydrogel pore networks facilitate the transport of H$_2$O$_2$ to the metal within the polymer matrix, thereby enhancing activity in dye degradation [51]. Furthermore, Table 5
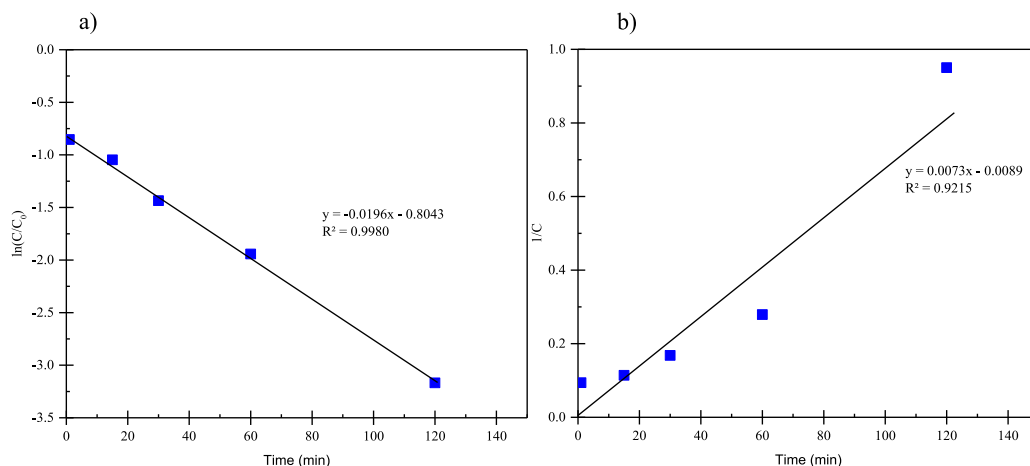

Fig. 11. Kinetics model methyl orange degradation of a) pseudo-first and b) pseudo-second-order reactions. (For interpretation of the references to color in this figure legend, the reader is referred to the Web version of this article.)

Table 3

Kinetic study for MO degradation over Fenton-like reaction.

Pseudo first order model		Pseudo second order model	
k_1 [1/min]	R^2	k_2 [L/(mg·min)]	R^2
0.0196	0.9980	0.0073	0.9215

Table 4

Cost estimation for Fenton-like Reaction of Methyl Orange under the suggested condition.

Item	Value	Unit cost (USD per kg)	Combined cost ($)
Synthesis of Cu–Fe	0.5 M FeCl$_3$·6H$_2$O	59.25	0.08
	0.1 M CuCl$_2$·2H$_2$O	68.65	0.01
	0.2 M FeSO$_4$·7H$_2$O	31.27	0.02
	5.0 M NaOH	10.66	0.26
	EtOH	17.85	0.89
	0.4 g Cu–Fe	–	1.26
Synthesis of catalyst bead	0.75 g Cu–Fe	–	2.36
	1.00 g Sodium Alginate	7.98	0.01
	0.3 M CaCl$_2$·2H$_2$O	24.71	0.12
	1.2 g [0.75-(Cu–Fe)/Alg]	–	2.49
Reaction cost per 1 L of Methyl orange (25 mg/L)	2 g [0.75-(Cu–Fe)/Alg]	–	4.15
	100 mM (30 % H$_2$O$_2$)	0.004	0.05
	0.01 M (NaOH)	10.66	–
Total			4.20

Table 5

Comparative Performance of [0.75-(Cu–Fe)/Alg] Bead and Bare Cu–Fe powder.

Catalyst	Cycles	Weight of catalyst (mg)		MO removal (%)	Metal leaching (mg)		[a]ALMW (mg)	CWA (mg)	ACWL (%)
		Fresh	Spent		Fe	Cu			
0.75-(Cu–Fe)/Alg	1st	200	178	97.67	0.082	0	0.082	178	11.0
	2nd	178	164	82.48	0.061	0	0.143	164	18.9
	3rd	164	154	75.77	0.051	0	0.194	154	25.0
	4th	154	147	54.53	0.051	0	0.245	147	29.5
Cu–Fe powder	1st	100	77	45.01	0.133	0.325	0.458	77	23.0
	2nd	77	63	51.63	0.123	0.301	0.882	63	37.0
	3rd	63	51	50.93	0.113	0.271	1.266	51	49.0
	4th	51	40	33.14	0.102	0.253	1.621	40	60.0

CWA is the catalyst weight after reaction (mg).
ACWA is the Accumulation of catalyst weight after reaction (mg).
ALMW is the Accumulation of leached metal weight (mg).
ACWL is the Accumulation of catalyst weight loss (%).
[a] Weight of leached metal after reaction.

shows that Cu–Fe powder's leached metal content was higher than 0.75-(Cu–Fe)/Alg. Cu–Fe powder had approximately 0.458 mg of leached metal, whereas 0.75-(Cu–Fe)/Alg had around 0.082 mg. These results indicate that encapsulating the metal within alginate significantly reduces copper leaching into the solution. Additionally, the leached iron content was lower in the 0.75-(Cu–Fe)/Alg compared to the Cu–Fe powder. Thus, alginate enhances stability by reducing metal leaching. For reusability, we found that the catalyst activity of Cu–Fe powder decreased from 45 % to 33 % due to the leached metal and mass loss in each cycle, causing the decreasing performance in each cycle. Besides, the mass loss was exhibited at about 60 % in the fourth cycle because the mass loss occurs during the separating, washing, and drying process. Regarding reusability, we found that the catalytic activity of Cu–Fe powder decreased from 45 % to 33 % over successive cycles due to metal leaching and mass loss. In each cycle, leached iron and copper metals were approximately 0.11 mg (1.1 mg/L) and 0.29 mg (2.9 mg/L), respectively, contributing to the performance reduction. Additionally, by the fourth cycle, the cumulative mass loss reached about 60 %; the loss occurred from two causes: firstly, the metal leaching was around 0.3 %, and the other one was the separation, washing, and drying processes before reusing the catalyst. Nonetheless, 0.75-(Cu–Fe)/Alg exhibited a similar trend, with catalytic activity decreasing from 97 % to 54 % over successive cycles. However, the leached iron was only about 0.06 mg (0.6 mg/L), and no leached copper was observed after the reaction. This highlights the novelty of alginate in inhibiting copper leaching into the solution during successive cycles. Additionally, the cumulative mass loss for 0.75-(Cu–Fe)/Alg was about 30 %, which is half that of Cu–Fe powder. The mass loss occurred due to three primary reasons: metal leaching, which accounted for around 0.12 %, and the separation, washing, and drying processes before reusing the catalyst. Despite these processes, 0.75-(Cu–Fe)/Alg experienced significantly lower mass loss compared to Cu–Fe powder.

Moreover, our research provides insight into catalyst deactivation after successive reaction cycles. FTIR analysis was employed to

observe changes in the functional groups of the catalyst beads. The FTIR spectra of 0.75-(Cu–Fe)/Alg for fresh and first-spent catalysts showed no major changes, as most peaks maintained the same position and width. Fig. 12 shows that the C–O–O and C–O–C peaks slightly shrank in successive cycles. This phenomenon occurred from the Fenton-like reaction that produced radical oxidizers that broke down the polymer chains of alginate into smaller fragments through oxidative cleavage of the polymer backbone. Moreover, the C–O–O group, indicative of polymer cross-linkage, showed a decrease, implying reduced cross-linking. Therefore, catalyst deactivation was due to depolymerization, and with further successive runs, catalytic activity significantly decreased.

However, our investigation revealed that the leaching of iron metal during the process exceeded the World Health Organization (WHO) standard limit of 0.3 mg/L. So, it is crucial to implement additional methods to reduce leached iron metal, such as precipitation techniques. This method entails the recovery of metal ions from the solution by inducing their precipitation in an alkaline environment, typically at a pH of around 10. Subsequently, the precipitated metal can be reclaimed and repurposed for other processes, promoting sustainability and minimizing environmental impact before the discharge of the treated water.

A comparative analysis of catalytic performance between 0.75-(Cu–Fe)/Alg and other related studies, as depicted in Table 6, further supports the effectiveness of the Fenton-like system, particularly noteworthy for its compatibility with neutral pH and high activity efficiency of 97 % in MO removal. In contrast to the homogeneous catalyst (Fe^{2+}/Fe^{3+}), which exhibited a similar efficiency of approximately 97 %, the homogeneous catalyst requires a further process to remove iron sludge from the process. Our work demonstrates reusability for subsequent runs, although the catalyst's activity slightly decreased in successive cycles. Moreover, this study still achieves a high activity level with MO removal up to 97 % compared to the heterogeneous catalyst. This underscores the significance of conducting the reaction at a neutral pH, showcasing the catalyst's capability to degrade MO in solution, which the other studies still work at acid pH.

3.8. Plausible catalytic mechanisms

The degradation mechanism of methyl orange via a Fenton-like reaction employing catalyst beads, with Ca as a cross-linker for the polymer encapsulating Cu and Fe metals, was elucidated. Upon the addition of H_2O_2, •OH generation ensued. Fe and Cu metals cooperatively underwent Fenton-like reactions to produce radicals, as illustrated in Equations (4)–(7). Furthermore, Cu–Fe augmented the metal synergistic effect between Cu and Fe, enhancing their catalytic activity, as indicated by Equation (8) [23].

$$Fe^{2+} + H_2O_2 \rightarrow Fe^{3+} + \bullet OH + OH^- \tag{4}$$

$$Fe^{3+} + H_2O_2 \rightarrow Fe^{2+} + \bullet OOH + H^+ \tag{5}$$

$$Cu^+ + H_2O_2 \rightarrow Cu^{2+} + \bullet OH + OH^- \tag{6}$$

$$Cu^{2+} + H_2O_2 \rightarrow Cu^+ + \bullet OOH + H^+ \tag{7}$$

$$Fe^{3+} + Cu^+ \rightarrow Fe^{2+} + Cu^{2+} \tag{8}$$

As pH levels increased, Fe activity decreased due to the elevated formation of Fe^{3+} ions, as described in Equation (4). Conversely, Cu demonstrated enhanced performance at higher pH levels, undergoing oxidation to produce Cu^{2+}, as depicted in Equations (6) and (7). Additionally, Cu^+ and Fe^{3+} engaged in redox reactions, facilitating continuous redox cycles between Fe^{3+}/Fe^{2+} and Cu^+/Cu^{2+} pairs in 0.75-(Cu–Fe)/Alg, favoring Fenton-like reactions. Consequently, more H_2O_2 reacted with active sites, leading to increased OH• radical production, as outlined in subsequent equations. This catalyst system effectively promoted the mutual enhancement of Cu and Fe metals, supported by alginate, which mitigated metal leaching. Moreover, alginate assistance significantly improved the catalytic
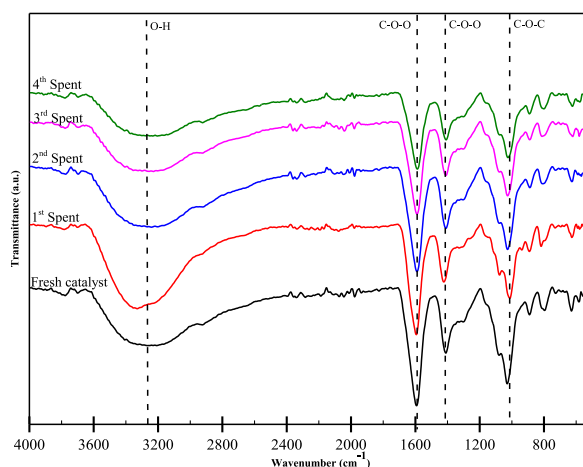

Fig. 12. FTIR spectra of 0.75-(Cu–Fe)/Alg in reused catalyst.

Table 6

Comparison of methyl orange removal via Fenton-like reaction.

Catalyst	Condition	Removal (%)	Reference
Fe^{2+}/Fe^{3+}	MO 18 mg/L, Catalyst load of 0.05 g/L, pH 2.8, $[H_2O_2]$ 2.93 mM, and 15 min	97.80	[49]
Goethite	MO 75 mg/L, Catalyst load of 0.30 g/L, pH 3.0, $[H_2O_2]$ 3.88 mM, and 30 min	94.80	[52]
$NiFe(C_2O_4)_x$	MO 20 mg/L, Catalyst load of 0.40 g/L, pH 6.2, $[H_2O_2]$ 10 mM and 30 min	98.00	[53]
Fe–Mn/MCM-41	MO 100 mg/L Catalyst load of 1.00 g/L, pH 3.0, $[H_2O_2]$ 5 mM and 120 min	100.00	[54]
0.75-(Cu–Fe)/Alg	MO 25 mg/L, Catalyst load of 2.00 g/L, pH 7.0, $[H_2O_2]$ 100 mM and 120 min	97.67	This work

efficiency of the reaction, resulting in enhanced radical production. Upon completion of these reactions, radicals facilitated the degradation of methyl orange into H_2O and CO_2.

4. Conclusion

In summary, this study depicts a significant leap forward in the heterogenous catalysis for Fenton-like reactions—the superiority of bimetal catalysts over singular metal components in facilitating MO degradation. The synthesis of Cu–Fe powder was prepared through co-precipitation and was encapsulated within alginate via the hydrogel method. The synergistic effect between Cu and Fe integrated with sodium alginate resulted in significantly enhanced catalytic activity and extended efficacy across a neutral pH, highlighting its potential for practical applications. The alginate-based polymer reduces the leached metal and improves the catalytic activity. Moreover, the kinetic study of 0.75-(Cu–Fe)/Alg has been fitted in the pseudo-first-order reaction, with a rate constant of 0.0196 min^{-1}. By systematically investigating the influence of pH variation, metal loading ratios, and H_2O_2 dosage, the suggested conditions led to an impressive MO removal efficiency of approximately 97 %. Additionally, catalyst deactivation stemming from depolymerization was displayed as the breaking down of the polymer bond. To mitigate this issue, the polymer could be enhanced through composite modification. These findings contribute to the fundamental understanding of heterogeneous catalysis and offer a promising solution for efficient and sustainable wastewater treatment. Besides, the wastewater treatment cost is $4.20 per liter for MO (25 mg/L) removal over a Fenton-like process. The less Fe leaching and ease of recyclability of Cu–Fe/Alg catalysts position them as attractive candidates for addressing water pollution challenges on a larger scale, emphasizing their potential impact on real-world applications.

Data availability statement

The authors confirm that the data supporting the findings of this study are available within the article.

CRediT authorship contribution statement

Pongpanit Kongkoed: Writing – review & editing, Writing – original draft, Validation, Methodology, Investigation, Conceptualization. **Natthaphong Lertna:** Methodology, Investigation. **Pakpoom Athikaphan:** Methodology, Investigation. **Athit Neramittagapong:** Writing – review & editing, Validation, Supervision, Methodology, Conceptualization. **Sutasinee Neramittagapong:** Writing – review & editing, Validation, Supervision, Resources, Methodology, Conceptualization.

Declaration of competing interest

The authors declare that they have no known competing financial interests or personal relationships that could have appeared to influence the work reported in this paper.

Acknowledgments

References

[1] I. Khan, K. Saeed, I. Zekker, B. Zhang, A.H. Hendi, A. Ahmad, et al., Review on methylene blue: its properties, Uses, toxicity and Photodegradation, Water (Switzerland) 14 (2022), https://doi.org/10.3390/w14020242.

[2] A.U. Khan, M. Zahoor, M.U. Rehman, A.B. Shah, I. Zekker, F.A. Khan, et al., Biological mineralization of methyl orange by Pseudomonas aeruginosa, Water (Switzerland) 14 (2022), https://doi.org/10.3390/w14101551.

[3] U. Habiba, T.A. Siddique, T.C. Joo, A. Salleh, B.C. Ang, A.M. Afifi, Synthesis of chitosan/polyvinyl alcohol/zeolite composite for removal of methyl orange, Congo red and chromium (VI) by flocculation/adsorption, Carbohydr. Polym. 157 (2017) 1568–1576, https://doi.org/10.1016/j.carbpol.2016.11.037.

[4] D. Ramutshatsha-Makhwedzha, A. Mavhungu, M.L. Moropeng, R. Mbaya, Activated carbon derived from waste orange and lemon peels for the adsorption of methyl orange and methylene blue dyes from wastewater, Heliyon 8 (2022) e09930, https://doi.org/10.1016/j.heliyon.2022.e09930.

[5] D. Feng, A. Soric, O. Boutin, Treatment technologies and degradation pathways of glyphosate: a critical review, Sci. Total Environ. 742 (2020) 140559, https://doi.org/10.1016/J.SCITOTENV.2020.140559.

[6] I.A. Saleh, N. Zouari, M.A. Al-Ghouti, Removal of pesticides from water and wastewater: chemical, physical and biological treatment approaches, Environ. Technol. Innov. 19 (2020) 101026, https://doi.org/10.1016/J.ETI.2020.101026.

[7] S. Ziembowicz, M. Kida, Limitations and future directions of application of the Fenton-like process in micropollutants degradation in water and wastewater treatment: a critical review, Chemosphere 296 (2022), https://doi.org/10.1016/j.chemosphere.2022.134041.

[8] V. Kumar, T. Mohapatra, S. Dharmadhikari, P. Ghosh, A review paper on heterogeneous fenton catalyst: types of preparation, modification techniques, factors affecting the synthesis, characterization, and application in the wastewater treatment, Bull. Chem. React. Eng. Catal. 15 (2020) 1–34, https://doi.org/10.9767/bcrec.15.1.4374.1-34.

[9] A. Shokri, M.S. Fard, A critical review in Fenton-like approach for the removal of pollutants in the aqueous environment, Environmental Challenges 7 (2022), https://doi.org/10.1016/j.envc.2022.100534.

[10] P. Athikaphan, K. Wongsanga, S. Klanghiran, N. Lertna, A. Neramittagapong, S.C. Rood, et al., Degradation of formaldehyde by photo-Fenton process over n-ZVI/TiO2 catalyst, Environ. Sci. Pollut. Control Ser. 30 (2023) 90397–90409, https://doi.org/10.1007/s11356-023-25812-0.

[11] R. Raj, A. Tripathi, S. Das, M.M. Ghangrekar, Waste coconut shell-derived carbon monolith as an efficient binder-free cathode for electrochemical advanced oxidation treatment of endocrine-disrupting compounds, J. Environ. Manag. 348 (2023), https://doi.org/10.1016/j.jenvman.2023.119328.

[12] R. Raj, A. Tripathi, S. Das, M.M. Ghangrekar, Is waste-derived catalyst mediated electro-Fenton a sustainable option for mitigating emerging contaminants from wastewater? Curr Opin Environ Sci Health 37 (2024) https://doi.org/10.1016/j.coesh.2023.100523.

[13] M.S.F. Santos, A. Alves, L.M. Madeira, Paraquat removal from water by oxidation with Fenton's reagent, Chem. Eng. J. 175 (2011) 279–290, https://doi.org/10.1016/j.cej.2011.09.106.

[14] S. Das, R. Raj, M.M. Ghangrekar, Efficient algal lipid extraction via a green bio-electro-Fenton process and its conversion into biofuel and bioelectricity with concurrent wastewater treatment in a photosynthetic microbial fuel cell, Green Chem. 25 (2023) 7166–7182, https://doi.org/10.1039/d3gc01548c.

[15] R. Raj, S.M. Sathe, S. Das, M.M. Ghangrekar, Nickel–iron-driven heterogenous bio-electro-fenton process for the degradation of methylparaben, Chemosphere 341 (2023) 139989, https://doi.org/10.1016/J.CHEMOSPHERE.2023.139989.

[16] S. Rahim Pouran, A.A. Abdul Raman, W.M.A. Wan Daud, Review on the application of modified iron oxides as heterogeneous catalysts in Fenton reactions, J. Clean. Prod. 64 (2014) 24–35, https://doi.org/10.1016/J.JCLEPRO.2013.09.013.

[17] S. Hussain, E. Aneggi, D. Goi, Catalytic activity of metals in heterogeneous Fenton-like oxidation of wastewater contaminants: a review, Environ. Chem. Lett. 19 (2021) 2405–2424, https://doi.org/10.1007/s10311-021-01185-z.

[18] L. Singh, P. Rekha, S. Chand, Cu-impregnated zeolite Y as highly active and stable heterogeneous Fenton-like catalyst for degradation of Congo red dye, Sep. Purif. Technol. 170 (2016) 321–336, https://doi.org/10.1016/j.seppur.2016.06.059.

[19] D. Li, T. Yang, Y. Li, Z. Liu, W. Jiao, Facile and green synthesis of highly dispersed tar-based heterogeneous Fenton catalytic nanoparticles for the degradation of methylene blue, J. Clean. Prod. 246 (2020), https://doi.org/10.1016/j.jclepro.2019.119033.

[20] E. Aneggi, A. Trovarelli, D. Goi, Degradation of phenol in wastewaters via heterogeneous Fenton-like Ag/CeO2 catalyst, J. Environ. Chem. Eng. 5 (2017) 1159–1165, https://doi.org/10.1016/j.jece.2017.01.042.

[21] P. Sriprom, S. Neramittagapong, C. Lin, A. Neramittagapong, P. Assawasaengrat, Lignin removal from synthetic wastewater via Fenton-like reaction over Cu supported on MCM-41 derived from bagasse: optimization and reaction intermediates, Heliyon (2023) e13157, https://doi.org/10.1016/j.heliyon.2023.e13157.

[22] S. Ziembowicz, M. Kida, Limitations and future directions of application of the Fenton-like process in micropollutants degradation in water and wastewater treatment: a critical review, Chemosphere 296 (2022), https://doi.org/10.1016/j.chemosphere.2022.134041.

[23] T.B. Nguyen, C Di Dong, C.P. Huang, C.W. Chen, S.L. Hsieh, S. Hsieh, Fe-Cu bimetallic catalyst for the degradation of hazardous organic chemicals exemplified by methylene blue in Fenton-like reaction, J. Environ. Chem. Eng. 8 (2020), https://doi.org/10.1016/j.jece.2020.104139.

[24] Y. Wang, H. Zhao, G. Zhao, Iron-copper bimetallic nanoparticles embedded within ordered mesoporous carbon as effective and stable heterogeneous Fenton catalyst for the degradation of organic contaminants, Appl. Catal., B 164 (2015) 396–406, https://doi.org/10.1016/j.apcatb.2014.09.047.

[25] Q. Wu, M.S. Siddique, W. Yu, Iron-nickel bimetallic metal-organic frameworks as bifunctional Fenton-like catalysts for enhanced adsorption and degradation of organic contaminants under visible light: kinetics and mechanistic studies, J. Hazard Mater. 401 (2021), https://doi.org/10.1016/j.jhazmat.2020.123261.

[26] S. Karthikeyan, M.P. Pachamuthu, M.A. Isaacs, S. Kumar, A.F. Lee, G. Sekaran, Cu and Fe oxides dispersed on SBA-15: a Fenton type bimetallic catalyst for N,N-diethyl-p-phenyl diamine degradation, Appl. Catal., B 199 (2016) 323–330, https://doi.org/10.1016/j.apcatb.2016.06.040.

[27] R.A. Ramli, Slow release fertilizer hydrogels: a review, Polym. Chem. 10 (2019) 6073–6090, https://doi.org/10.1039/c9py01036j.

[28] R. Davarnejad, Z.R. Hassanvand, S. Mansoori, J.F. Kennedy, Metronidazole elimination from wastewater through photo-Fenton process using green-synthesized alginate-based hydrogel coated bimetallic iron-copper nanocomposite beads as a reusable heterogeneous catalyst, Bioresour. Technol. Rep. 18 (2022), https://doi.org/10.1016/j.biteb.2022.101068.

[29] S. Ben Ayed, L. Mansour, V. Vaiano, A. Halim Harrath, F. Ayari, L. Rizzo, Magnetic Fe3O4-natural iron ore/calcium alginate beads as heterogeneous catalyst for Novacron blue dye degradation in water by (photo)Fenton process, J. Photochem. Photobiol. Chem. 438 (2023) 114566, https://doi.org/10.1016/j.jphotochem.2023.114566.

[30] H. Hu, H. Zhang, Y. Chen, Y. Chen, L. Zhuang, H. Ou, Enhanced photocatalysis degradation of organophosphorus flame retardant using MIL-101(Fe)/persulfate: effect of irradiation wavelength and real water matrixes, Chem. Eng. J. 368 (2019) 273–284, https://doi.org/10.1016/j.cej.2019.02.190.

[31] J. Tang, J. Wang, MOF-derived three-dimensional flower-like FeCu@C composite as an efficient Fenton-like catalyst for sulfamethazine degradation, Chem. Eng. J. 375 (2019), https://doi.org/10.1016/j.cej.2019.122007.

[32] H. Liu, Y. Liu, X. Li, X. Zheng, X. Feng, A. Yu, Adsorption and fenton-like degradation of ciprofloxacin using corncob biochar-based magnetic iron–copper bimetallic nanomaterial in aqueous solutions, Nanomaterials 12 (2022), https://doi.org/10.3390/nano12040579.

[33] M. Thommes, B. Smarsly, M. Groenewolt, P.I. Ravikovitch, A.V. Neimark, Adsorption hysteresis of nitrogen and argon in pore networks and characterization of novel micro- and mesoporous silicas, Langmuir 22 (2006) 756–764, https://doi.org/10.1021/la051686h.

[34] K.A. Cychosz, M. Thommes, Progress in the physisorption characterization of nanoporous gas storage materials, Engineering 4 (2018) 559–566, https://doi.org/10.1016/j.eng.2018.06.001.

[35] M. Thommes, K. Kaneko, A.V. Neimark, J.P. Olivier, F. Rodriguez-Reinoso, J. Rouquerol, et al., Physisorption of gases, with special reference to the evaluation of surface area and pore size distribution (IUPAC Technical Report), Pure Appl. Chem. 87 (2015) 1051–1069, https://doi.org/10.1515/pac-2014-1117.

[36] L. Zhu, X. Zhang, L. Ran, H. Zhang, Y. Zheng, C. Liu, et al., Tri-modified ferric alginate gel with high regenerative properties catalysts for efficient degradation of rhodamine B, Carbohydr. Polym. 322 (2023), https://doi.org/10.1016/j.carbpol.2023.121309.

[37] W. Pi, L. Wu, J. Lu, X. Lin, X. Huang, Z. Wang, et al., A metal ions-mediated natural small molecules carrier-free injectable hydrogel achieving laser-mediated photo-Fenton-like anticancer therapy by synergy apoptosis/cuproptosis/anti-inflammation, Bioact. Mater. 29 (2023) 98–115, https://doi.org/10.1016/j.bioactmat.2023.06.018.

[38] P.K. Raul, R.R. Devi, I.M. Umlong, S. Banerjee, L. Singh, M. Purkait, Removal of fluoride from water using iron oxide-hydroxide nanoparticles, J. Nanosci. Nanotechnol. 12 (2012) 3922–3930, https://doi.org/10.1166/jnn.2012.5870.

[39] S.K. Shinde, D.P. Dubal, G.S. Ghodake, P. Gomez-Romero, S. Kim, V.J. Fulari, Influence of Mn incorporation on the supercapacitive properties of hybrid CuO/Cu(OH)2 electrodes, RSC Adv. 5 (2015) 30478–30484, https://doi.org/10.1039/c5ra01093d.

[40] G. Ch, Essential metal-based nanoparticles (Copper/Iron NPs) as potent nematicidal agents against Meloidogyne spp, Journal of Nanotechnology Research 1 (2019) 44–58, https://doi.org/10.26502/fjnr.004.

[41] A. Varughese, R. Kaur, P. Singh, Green synthesis and characterization of copper oxide nanoparticles using psidium guajava leaf extract, IOP Conf. Ser. Mater. Sci. Sci. Eng. 961 (2020), https://doi.org/10.1088/1757-899X/961/1/012011. IOP Publishing Ltd.

[42] L. Das, P. Das, A. Bhowal, Synthesis and application of alginate-nanocellulose composite beads for defluoridation process in a batch and fluidized bed reactor, J. Environ. Manag. 344 (2023), https://doi.org/10.1016/j.jenvman.2023.118569.

[43] L.Z. Liu, R. Zhou, Y.L. Li, Y.H. Pang, X.F. Shen, J. Liu, Covalent organic framework-sodium alginate-Ca2+-polyacrylic acid composite beads for convenient dispersive solid-phase extraction of neonicotinoid insecticides in fruit and vegetables, Food Chem. 441 (2024), https://doi.org/10.1016/j. foodchem.2024.138357.

[44] M. Zhang, K. Yi, X. Zhang, P. Han, W. Liu, M. Tong, Modification of zero valent iron nanoparticles by sodium alginate and bentonite: enhanced transport, effective hexavalent chromium removal and reduced bacterial toxicity, J. Hazard Mater. 388 (2020), https://doi.org/10.1016/j.jhazmat.2019.121822.

[45] N. Wang, B. Wang, Y. Wan, B. Gao, V.D. Rajput, Alginate-based composites as novel soil conditioners for sustainable applications in agriculture: a critical review, J. Environ. Manag. 348 (2023), https://doi.org/10.1016/j.jenvman.2023.119133.

[46] B. Ozbey Unal, Z. Bilici, N. Ugur, Z. Isik, E. Harputlu, N. Dizge, et al., Adsorption and Fenton oxidation of azo dyes by magnetite nanoparticles deposited on a glass substrate, J. Water Proc. Eng. 32 (2019), https://doi.org/10.1016/j.jwpe.2019.100897.

[47] Abdur-Rahim A. Giwa IABABOOSBTAS. Kinetic and Thermodynamic Studies of Fenton Oxidative Decolorization of Methylene Blue | Enhanced Reader n.d.

[48] M.K. Zhang, X.H. Ling, X.H. Zhang, G.Z. Han, A novel alginate/PVA hydrogel -supported Fe_3O_4 particles for efficient heterogeneous Fenton degradation of organic dyes, Colloids Surf. A Physicochem. Eng. Asp. 652 (2022), https://doi.org/10.1016/j.colsurfa.2022.129830.

[49] N.A. Youssef, S.A. Shaban, F.A. Ibrahim, A.S. Mahmoud, Degradation of methyl orange using Fenton catalytic reaction, Egyptian Journal of Petroleum 25 (2016) 317–321, https://doi.org/10.1016/j.ejpe.2015.07.017.

[50] Ibrahim Raheb MSM. Kinetic and Thermodynamic Studies of the Degradation of Methylene Blue by Photo-Fenton Reaction n.d.

[51] S. Cheng, C. Zhang, J. Li, X. Pan, X. Zhai, Y. Jiao, et al., Highly efficient removal of antibiotic from biomedical wastewater using Fenton-like catalyst magnetic pullulan hydrogels, Carbohydr. Polym. 262 (2021), https://doi.org/10.1016/j.carbpol.2021.117951.

[52] Y. Wang, Y. Gao, L. Chen, H. Zhang, Goethite as an efficient heterogeneous Fenton catalyst for the degradation of methyl orange, Catal. Today 252 (2015) 107–112, https://doi.org/10.1016/j.cattod.2015.01.012.

[53] Y. Liu, G. Zhang, S. Chong, N. Zhang, H. Chang, T. Huang, et al., NiFe(C_2O_4)$_x$ as a heterogeneous Fenton catalyst for removal of methyl orange, J. Environ. Manag. 192 (2017) 150–155, https://doi.org/10.1016/j.jenvman.2017.01.064.

[54] X. Zhang, J. Dong, Z. Hao, W. Cai, F. Wang, Fe–Mn/MCM-41: preparation, characterization, and catalytic activity for methyl orange in the process of heterogeneous fenton reaction, Trans. Tianjin Univ. 24 (2018) 361–369, https://doi.org/10.1007/s12209-018-0122-1.